JOURNAL OF AIRCRAFT
Vol. 29, No. 4, July–Aug. 1992

Aerodynamic Forces on Noncircular Cross-Section Missile Forebodies

Brian E. Est* and H. F. Nelson†
University of Missouri—Rolla, Rolla, Missouri 65401

A numerical investigation is performed to develop the aerodynamic characteristics of forebodies with noncircular cross sections in supersonic cruise. A robust, second order accurate Euler code, is utilized to determine C_L, C_D, and C_M for forebodies with circular, square, diamond, triangle, and inverted triangle cross sections. The predictions at Mach 2.01 compare well with wind tunnel data for angles of attack from 0 to 6 deg. Computed results at Mach 3.0 show that distinct aerodynamic advantages may be obtained by using forebodies with noncircular cross sections. In supersonic cruise, forebodies with noncircular cross sections develop considerably greater lift and lift/drag ratios than forebodies with circular cross sections.

Nomenclature

a = shape factor
a' = shape factor parameter (see Appendix)
C_D = drag coefficient, $D/q_\infty S$
$C_{D\text{wave}}$ = inviscid wave drag coefficient
C_L = lift coefficient, $L/q_\infty S$
C_M = pitching moment coefficient, $M_y/q_\infty Sl$
C_N = normal force coefficient, $F_N/q_\infty S$
C_Z = axial force coefficient, $F_Z/q_\infty S$
D = drag force
F_N = normal force
F_Z = axial force
L = lift force
l = reference length for pitching moment coefficient
M = Mach number
M_y = pitching moment
q_∞ = dynamic pressure, $\frac{1}{2}\rho_\infty V_\infty^2$
P = pressure
P_∞ = freestream pressure
P_{surf} = surface pressure
R = radius of inscribed circle in the forebody base
R_f = fillet radius (see Appendix)
r = radial position normal to longitudinal axis
S = reference area for coefficients
Z = axial distance
α = angle of attack in degrees
ρ_∞ = freestream density
ϕ = angular position in the crossflow plane in degrees

Introduction

A SIGNIFICANT amount of work has been published regarding forces and moments of tactical missiles with traditional circular cross-section fuselages. However, circular cross-sectional shapes do not make optimal use of internal storage volume allotted for munitions, nor cross-sectional area in launchers. Aboard today's ships and aircraft, space is a premium; therefore, efficient packaging of ordnance and usage of launcher volume is essential. This need has led to investigation of unorthodox body cross-sectional shapes. Some numerical[1,2] and experimental[3–8] work exists for missiles with noncircular cross-section fuselages. This paper presents results of an investigation of aerodynamic forces and moments for missile forebodies that have square, diamond, inverted triangular, and triangular cross-sectional shapes in supersonic cruise. The objective of this research is to upgrade the preliminary design data base to include these shapes.

The traditional approach to preliminary design has been to use a variety of analytical, empirical, and numerical methods to predict and evaluate missile configurations before the missile is constructed. The preliminary design process is iterative; therefore, quick, accurate methods are desirable. Analytical and empirical methods are generally the easiest to apply because the solutions can be obtained from hand calculations. Numerical analysis has grown in popularity due to 1) advances in high speed, digital computer technology, 2) ever-improving numerical algorithms, 3) ease of modification, and 4) application to a broad range of conditions and configurations.

Ideally, a full three-dimensional Navier-Stokes analysis should be used to determine the missile flowfield. This solution would provide the complete flowfield including boundary layer, skin friction, pressure distribution, and heat transfer. However, the Navier-Stokes equations require careful grid selection and fine meshes to resolve skin friction and heat transfer properly, because many Navier-Stokes solutions may be grid-dependent. The time required to study the gridding in addition to the large cost and large amount of computer time required for each solution is prohibitive in an iterative preliminary design analysis.

The Euler equations have been shown to give excellent results for missile aerodynamics[1–2] as well as other applications.[9–13] The pressure distribution given by the Euler equations is accurate for supersonic flow and can be integrated over the entire body to yield lift, wave drag, and moment data. Euler codes are not nearly as sensitive to gridding as the Navier-Stokes codes. The Euler equations convect vorticity and determine the circulation generated by shocks, but viscous phenomena, such as vortex shedding from the surface of smooth bodies, must be empirically modeled. Instead of flow separating and rolling up to form leeside vortices, inviscid calculations feature a strong crossflow shock which may generate sufficient vorticity to form leeside vortices.[14–21] However, the strength of these inviscid vortices is much smaller

Presented as Paper 91-0390 at the AIAA 29th Aerospace Sciences Meeting, Reno, NV, Jan. 7–10, 1991; received Feb. 2, 1991; revision received July 3, 1991; accepted for publication July 8, 1991.

*Graduate Student, Department of Mechanical and Aerospace Engineering and Engineering Mechanics; currently Aerospace Engineer, Dynetics, Inc., Huntsville, AL. Student Member AIAA.

†Professor of Aerospace Engineering, Thermal Radiative Transfer Group, Department of Mechanical and Aerospace Engineering and Engineering Mechanics. Associate Fellow AIAA.

than that of measured vortices and the predicted inviscid pressure distribution differs from the measured one.

Jorgensen[6] performed a wind tunnel flow visualization investigation of forebodies with noncircular cross section at Mach 1.98 and 3.88. Square and triangular body cross-sectional shapes with shape factors of 0.9748 and 0.9834 (see Appendix), respectively, were examined at angles of attack from 0 to 17 deg. At high angles of attack, the corners produced a leeside vortex system. Leeside vortices were most prevalent at angles of attack greater than 5 deg. Thus, an inviscid analysis should be satisfactory for angles of attack less than 5 deg. If leeside vortices are a primary constituent of the measured flowfield, inviscid computations will depart from wind tunnel data.

Method of Analysis

A numerical approach was used to determine the force and moment coefficients of forebodies in supersonic cruise. The shape of the forebodies in the crossflow plane makes the flowfield calculations computationally complex due to the sharp corners. ZEUS (Zonal EUler Solver), a finite volume Euler code,[22-25] was used to predict the lift, wave drag, and pitching moment data for this investigation. ZEUS was selected due to its robustness and second order accuracy. ZEUS gridding and results are discussed at length in Refs. 1 and 22–25. Good aerodynamic force prediction has been obtained using coarse meshes (24 × 24, r by ϕ). However, coarse meshes do not provide enough resolution to predict complex flowfields containing crossflow shocks and leeside vortices.

ZEUS is an axial marching code. The solutions begin at the missile nose, where a conical starting solution calculates the flowfield at the initial value plane located at $Z/R = 0.3$. The cross section of the nosecone is circular for $0 \leq Z/R \leq 0.3$. From $Z/R = 0.3$ to the nosecone/fuselage juncture at $Z/R = 14$, the nosecone is linearly tapered; it varies from the circular cross section to the desired fuselage shape linearly as a function of Z/R. For $Z/R \geq 14$ the cross section is constant.

All of the cross-sectional shapes investigated are related by a shape factor, a, which is derived and illustrated in the Appendix. As a varies from 0 to 1 it quantifies the cross-sectional shape. When $a = 0$, all shapes degenerate to a circular cross section. When $a = 1$, cross-sectional shapes become sharp cornered squares, diamonds, or triangles, depending upon the shape of interest.

All the numerical calculations were done on the IBM 4381 mainframe computer at the University of Missouri-Rolla. The ZEUS code was set up making use of pitch plane symmetry to reduce computer memory and run time. The numerical grid was configured to use a single zone with a simple 36 × 36 (r by ϕ), uniform mesh in each crossflow plane.

Code Validation

A comparison between calculated lift, drag, and pitching moment coefficient predictions and wind tunnel data from Carlson and Gapcynski[5] was performed to assess the accuracy of the numerical computations. The forebody dimensions and cross-sectional shapes which were tested are shown in Fig. 1.

Reference 5 contains experimental data for circular, square, triangular, and other cross-sectional shapes at Mach 2.01. The shape factors of the wind tunnel models were $a = 0.5580$ and 0.5122 for the square and the triangular cross sections, respectively. The data for the forebody model with diamond cross section was generated by rolling the square 45 deg. Likewise, the data for the inverted triangular cross section was generated by rolling the triangular cross section 60 deg.

The experimental nosecone was a tangent ogive, but it was not clear from Ref. 5 how the nosecone matched the fuselage shapes at the nosecone fuselage junction. The primary difference between the experimental and numerical flowfield solutions is the pressure distribution. The tangent ogive nosecone produces a constant expansion such that the pressure gradually recovers from the bow shock. The linearly

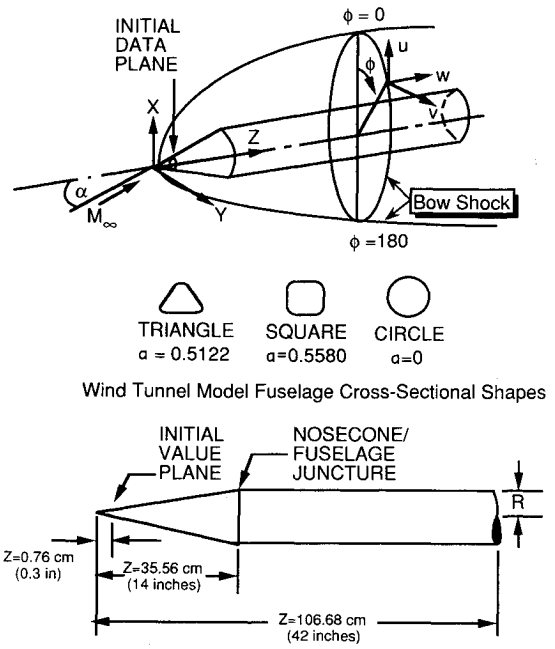

Wind Tunnel Model Fuselage Cross-Sectional Shapes

Fig. 1 ZEUS nomenclature and wind tunnel model data from Ref. 5. R = 5.08, 4.60, and 4.16 cm and a = 0.0, 0.5580, and 0.5122, for the circle, square, and triangle cross sections, respectively.

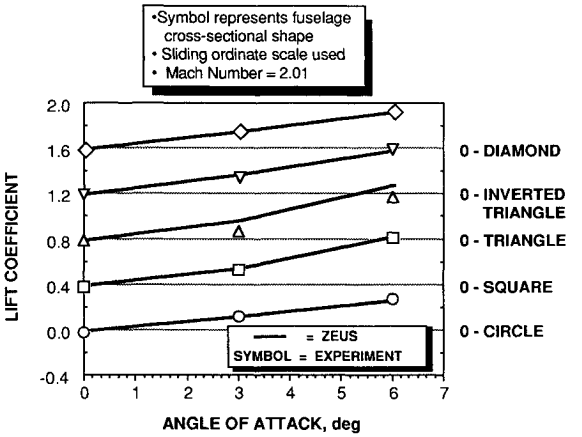

Fig. 2 Comparison of numerical and experimental (Ref. 5) lift coefficient.

tapered nosecone experiences virtually no pressure recovery up to the nosecone/fuselage juncture at which an expansion occurs. The difference between the nosecone shapes lead to a small difference in flowfields; however, it is assumed that this difference is negligible.

A comparison between numerical and experimental results for lift, drag, and pitching moment coefficient for forebodies with square, diamond, circular, inverted triangular, and triangular cross sections is shown in Figs. 2–4 vs angle of attack. The radius of the inscribed circle R was slightly different for each shape as given in the caption of Fig. 1. Consequently, the reference area for the coefficients was taken as 80.83 cm^2 for all the shapes.[5] Care must be taken in reading Figs. 2–4 because a sliding scale is used on the ordinate. To read the scale, choose the desired shape on the right and slide the scale up the ordinate so that the zeros correspond to the same horizontal hashmark. The shape of the symbols in Figs. 2–4 represent the shape of the forebody cross section.

Figure 2 shows the comparison for lift coefficient. The numerical results show excellent agreement with experiment throughout the range of angle of attack for all five shapes. The lift curve slope of the noncircular shapes is slightly greater than it is for the circle. Figure 3 presents the comparison for pitching moment coefficient. The moment is taken about a

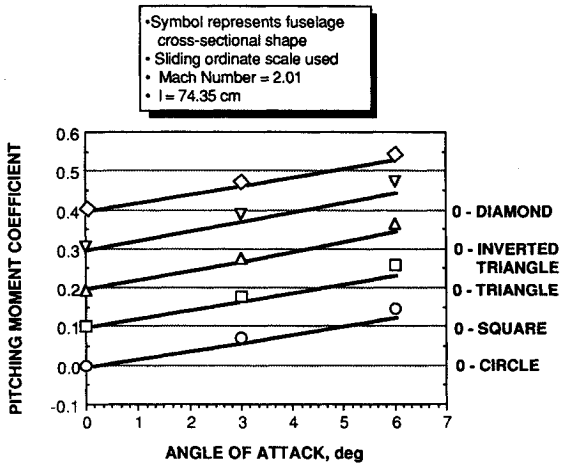

Fig. 3 Comparison of numerical and experimental (Ref. 5) pitching moment about a station 74.35 cm aft of the missile nosetip. Reference length l is 74.35 cm.

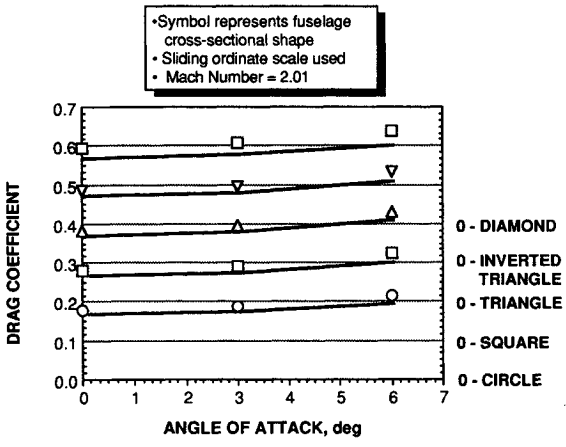

Fig. 4 Comparison of numerical and experimental (Ref. 5) total drag coefficient.

station 74.35 cm aft of the nosetip of the 106.68-cm-long forebody used in the tests, and it is positive nose-up. Again, the computed results compare well with experiment; however, they slightly undershoot the experimental data at higher angles of attack. The maximum difference is about 15%. The total experimental and numerical lift force is nearly identical; however, the distribution of the lift force is different because of the differences in the experimental and numerical nosecone shapes. Thus, the nosecones have slightly different center-of-pressure locations. The large moment arm in the pitching moment calculation accents this difference and leads to a slight difference between the predicted and experimental pitching moment.

A comparison between the calculated drag coefficient and experiment is shown in Fig. 4. The Euler code only predicts wave and pressure drag. Skin friction drag data from the USAF Automated Missile DATCOM was added to the drag predicted by ZEUS to estimate of the total drag coefficient.[26] This total drag coefficient is shown in Fig. 4. It provides a satisfactory preliminary design estimate of the total drag (excluding base drag). All of the data presented graphically in Figs. 2–4 is tabulated in Refs. 27 and 28.

Physics of the Flowfield

The cross-sectional shapes considered in this investigation cause several flowfield phenomena to occur. As a progresses from 0 to 1, the corners of the shape, whether it be square or triangular, jut out into the flow resulting in additional shocks—one at each corner. Figure 5 presents a profile sketch of the flowfield of two missiles: an $a = 0$ case (forebody with circular cross section) and an $a = 1$ case (forebody with diamond cross section). Both profiles are shown viewed from above. Recall that the noncircular shapes are built up surrounding an inscribed circle. When $a = 0$, the conical nosecone shape is extended to the nosecone/fuselage juncture at which an expansion occurs. When a is not zero, corners protrude into the flowfield. As the corner of the diamond juts out into the flow, a secondary oblique shock forms behind the bow shock. Consequently, these corners influence the pressure field on the forebody.

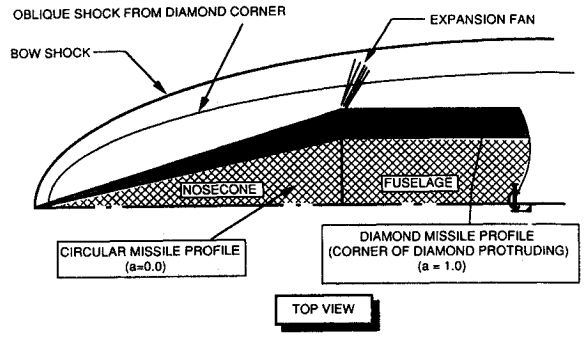

Fig. 5 Flowfield phenomena for circular and diamond cross sections (top view).

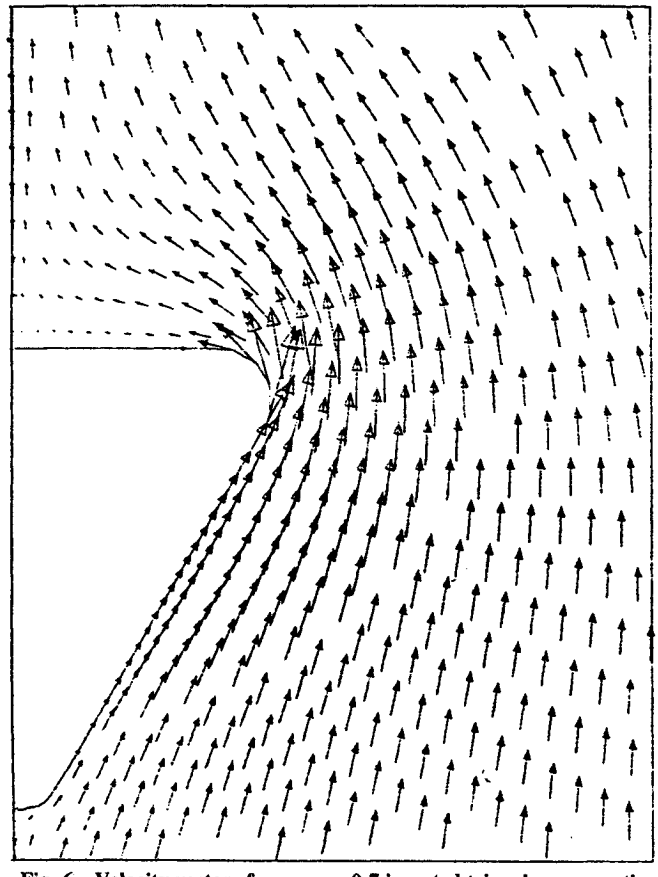

Fig. 6 Velocity vectors for an $a = 0.7$ inverted triangle cross section at $Z/R = 18$, for $M = 3$, $\alpha = 3$ deg.

The corners not only affect flow in the axial direction, but also affect flow in the crossflow plane. When the missile is at an angle of attack crossflow develops: flow moves upward from the windward side of the forebody (bottom) along the side of the forebody toward the leeward side (top). The corners of the forebody affect the characteristics of the crossflow. Figure 6 shows velocity vectors in the crossflow plane at $Z/R = 18$ for the inverted triangular cross section. The flow travels around the side of the forebody at a relatively steady rate. When the flow moves around the corner it reacts by expanding. In viscous flow, the flow usually separates and rolls up to form a leeside vortex at the corner. In inviscid

calculations, the expansion can result in a crossflow shock if the local speed of sound is exceeded.

Extended Numerical Results

We have shown that ZEUS predictions agree well with experiment. This section reports extended numerical results using the missile forebody model similar to that shown in Fig. 1, except the nosecone body junction is at $Z/R = 6.0$. Also, for this body the noncircular shapes are built around an inscribed circle of radius R ($R = 2.54$ cm). The area (πR^2) of this inscribed circle is used as the reference area for C_L, C_D, and C_M. This reference area was used to consistently reference the coefficients for all the shapes to the same area.

Surface Pressure

The surface pressure distribution is closely related to the physical nature of the crossflow. Figures 7 and 8 show the dimensionless surface pressure versus angular position at selected axial locations at $\alpha = 3$ deg and $M = 3$. Figure 7 presents the surface pressure distribution for a circular and diamond forebody. The smooth change in pressure distribution from the windward side ($\phi = 180$ deg) to the leeward side ($\phi = 0$ deg) is typical for a conventional circular cross section missile forebody. The sharp drop at $\phi = 90$ deg in the diamond cross section data shows the expansion of the crossflow as it travels around the corner from the windward to the leeward side. In addition, the diamond has an expansion at the windward corner on the nosecone (160 deg $\leq \phi \leq 180$ deg, $Z/R = 5$) due to the development of the lower corner of the diamond cross section along the nosecone. The corners of the diamond (located at $\phi = 180$, 90, and 0 deg) have a substantial effect on the pressure distribution. The expansion around the corners decreases the pressure on the leeward side of the forebody, ultimately increasing the lift generated by the body. Figure 8 shows similar trends for square and inverted triangle cross sections. The pressure distributions on the nosecone indicate a shock at ϕ just greater than the corner angle and an overexpansion as the flow moves around the corner. This trend gradually dissipates at larger Z/R values.

Figure 9 shows the dimensionless surface pressure versus axial position at 5 angular locations for the circular cross section. At $Z/R \leq 6$ (from the initial value plane to the nosecone/fuselage juncture) the pressure is nearly constant. At the nosecone/fuselage juncture ($Z/R = 6$) the effects of the linearly tapered nosecone are illustrated by the abrupt expansion. The pressure ratio drops due to the expansion, then it recovers to approximately 1 at the end of the forebody. This variation is typical for all the cross section shapes (see Refs. 27 and 28). Polhamus, Geller, and Grunwald[29] have published experimental and theoretical surface pressure distributions for noncircular, infinitely long cylinders in a cross flow. They considered square, diamond, and triangular shapes; however, the corners were not sharp. The present pressure distributions at $Z/R = 50$ show excellent agreement with those of Ref. 29.

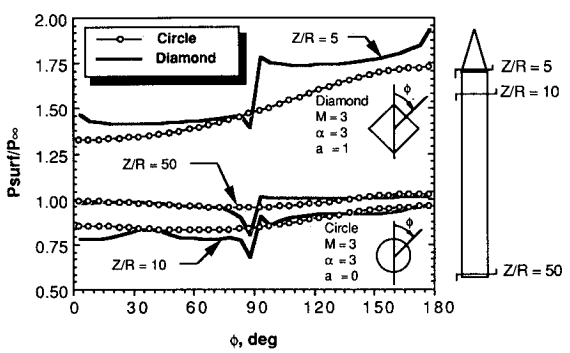

Fig. 7 Cross flow pressure distributions for a circular ($a = 0$) and diamond ($a = 1$) cross section for $M = 3$, $\alpha = 3$ deg.

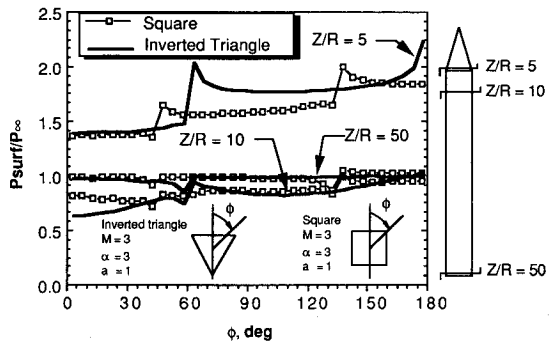

Fig. 8 Cross flow pressure distributions for a square, triangular, and inverted triangular cross section for $a = 1$, $M = 3$, $\alpha = 3$ deg.

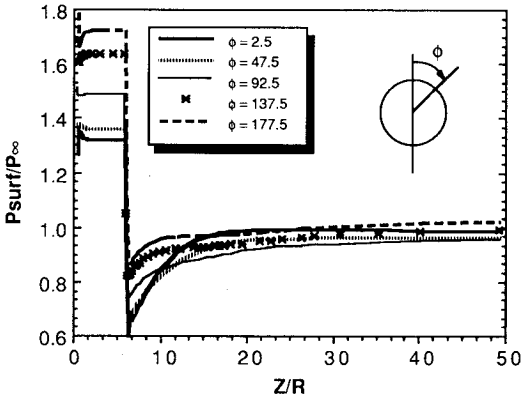

Fig. 9 Axial surface pressure distribution for a circular cross section for $M = 3$, $\alpha = 3$ deg.

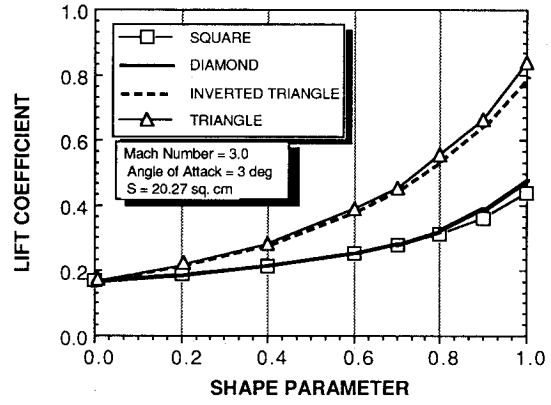

Fig. 10 Lift coefficient vs shape factor for $M = 3$, $\alpha = 3$ deg.

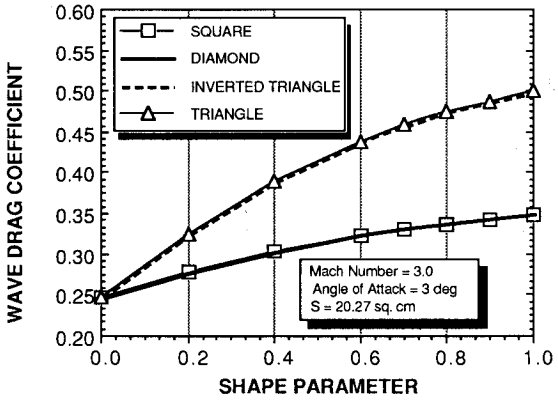

Fig. 11 Wave drag coefficient vs shape factor for $M = 3$, $\alpha = 3$ deg.

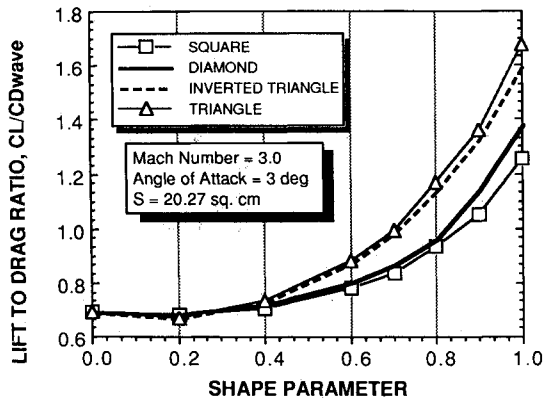

Fig. 12 Lift to wave drag ratio vs shape factor for $M = 3$, $\alpha = 3$ deg.

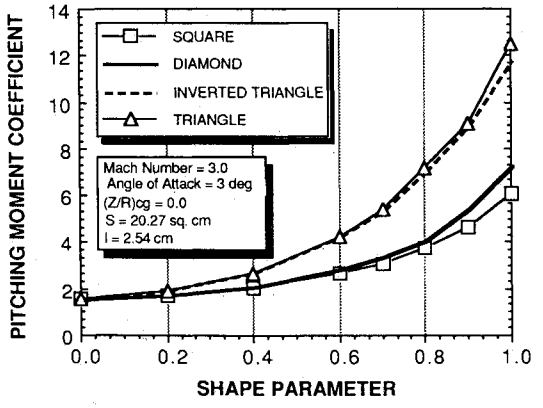

Fig. 13 Nose-down pitching moment coefficient about the nosetip vs shape factor for $M = 3$, $\alpha = 3$ deg. Reference length l is 2.54 cm.

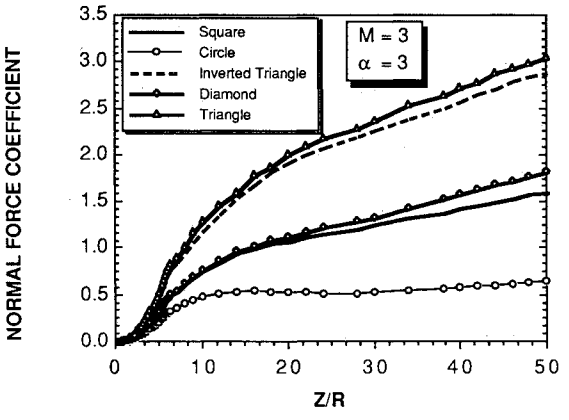

Fig. 14 Normal force coefficient vs axial length of the missile forebody for $a = 0$ (circle), $a = 1$ (other shapes), $M = 3$, $\alpha = 3$ deg.

Lift, Drag, and Moment Coefficient

This section presents the lift, wave drag, and pitching moment coefficient numerical results for the forebody cross sections as a function of shape factor for a forebody of length $Z/R = 40$. The calculations are for an angle of attack of 3 deg at Mach 3. Figure 10 shows the lift coefficient vs shape factor. For $a = 0$, all shapes are circles of radius R, and for $a = 1$, the shape of interest is sharp cornered. C_L, $C_{D_{wave}}$, and C_M are all based on the cross-sectional area of the inscribed circle (πR^2) inherent in all the shapes of this investigation. This reference area is constant for all shapes and all values of a. The triangular cross sections generate the largest C_L. The C_L for the squares is smaller than the C_L for the triangles. The diamond has a slightly larger C_L than the square. Both are larger than the baseline C_L of the circular cross section.

Figure 11 shows wave drag versus the shape factor for all five forebody shapes at Mach 3. Wave drag is proportional to cross-sectional area. At $a = 1$ the areas are $3\sqrt{3}R^2$, $4R^2$, and πR^2 for the triangles, squares, and circle, respectively. (Recall that $C_{D_{wave}}$ is defined using reference area πR^2.) The circular cross section has the smallest wave drag coefficient due to its small frontal area. The triangle shapes have higher wave drag than the square shapes because they have a larger frontal area.

Figure 12 shows the lift to wave drag ratio vs shape factor. This is an important parameter with respect to range. All the cross-sectional shapes produce higher lift to wave drag ratios than the circular forebody. The triangles produce the highest lift to wave drag ratios with the triangle being slightly larger than the inverted triangle. The square shapes produce smaller lift to wave drag ratios than the triangles with the diamond lift to wave drag being slightly larger than the square. The lift to total drag ratio can be calculated by multiplying L/D from Fig. 12 by the ratio of wave drag to total drag, where the total drag includes wave drag from Fig. 11 and viscous drag from any source.

Figure 13 shows the pitching moment about the nosetip versus shape factor with positive being nose-down. The reference length for C_M is R, the radius of the inscribed circle ($l = R = 2.54$ cm). The triangles produce the highest pitching moments with the squares generating slightly lower values. Pitching moment follows the trends in lift coefficient. The higher pitching moments of the noncircular shapes implies that they may need more pitch control power than circular shapes. All of these preceding lift, wave drag, and pitching moment coefficient data are tabulated in Refs. 27 and 28.

Effect of Fuselage Length

This section examines the effect of forebody length upon the normal and axial force coefficients and the pitching moment coefficient for all five shapes. Note that $a = 1$ for the triangle and square shapes, and $a = 0$ for the circular shape.

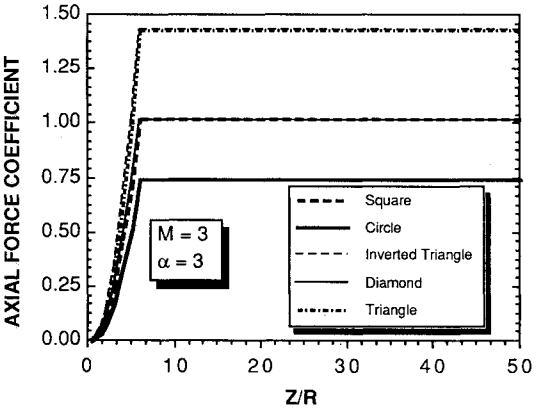

Fig. 15 Axial force coefficient vs axial length of the missile forebody for $a = 0$ (circle), $a = 1$ (other shapes), $M = 3$, $\alpha = 3$ deg.

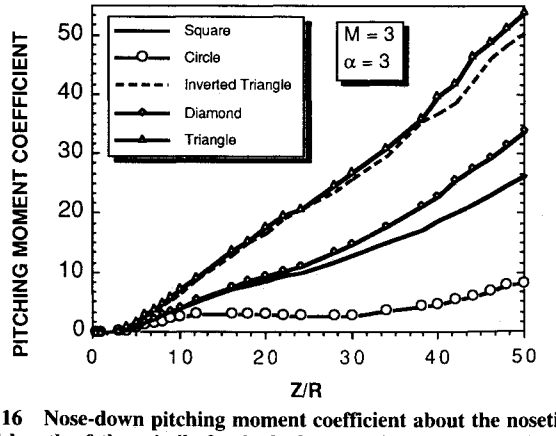

Fig. 16 Nose-down pitching moment coefficient about the nosetip vs axial length of the missile forebody for $a = 0$ (circle), $a = 1$ (other shapes), $M = 3$, $\alpha = 3$ deg. Reference length l is 2.54 cm.

Figure 14 shows the effect that body length has on the normal force coefficient. For all of the shapes, except the circle, the normal force coefficient is approximately linear with Z/R for $Z/R \geq 25$. The noncircular cross sections produce considerably more lift than the circular cross section for any length missile.

The axial force coefficient, at low angles of attack, is approximately equal to the wave drag. Wave drag is proportional to the cross-sectional area and, as is shown in Fig. 15, is constant for Z/R greater than 6 where the cross-sectional area of the forebodies becomes constant. The triangles have the largest wave drag, followed by the square shapes, with the circular shape having the smallest.

Figure 16 shows the effect of fuselage length on pitching moment. The moment coefficient is approximately linear with Z/R for $Z/R \geq 35$. It is directly proportional to C_N.

Summary and Conclusions

Numerical predictions of supersonic, noncircular cross section missile forebody lift, wave drag, and pitching moment using the three-dimensional Euler equations are shown to agree well with the experimental measurements of Carlson and Gapcynski[5] at small angles of attack (cruise flight) at Mach 2.01 for square and triangle cross sections with shape factors 0.5580 and 0.5122, respectively. Predictions of pitching moment trends also agree with experiment, but the effects of the difference between the linearly tapering nosecone used in the computations and the tangent ogive nosecone used in the wind tunnel models becomes important as angle of attack increases. This generally results in a slight underprediction of pitching moment at higher angles of attack. The combination of Euler equation, numerically predicted wave drag, and Missile DATCOM skin friction drag data, provide a total drag estimate (excluding base drag) which agrees with experiment and is suitable for preliminary design.

Aerodynamic characteristics of forebodies with square and triangular cross sections have been computed and compared with forebodies with a circular cross section at Mach 3 and an angle of attack of 3 deg. Predictions were made for forebodies with cross-sectional shapes ranging from a circle to sharp-cornered squares and triangles. Forebodies of progressively greater noncircularity develop higher values of lift, pitching moment, and lift/drag ratio than forebodies with circular cross section. These higher force and moment values are important factors in optimizing the range, determining the performance and sizing the control surfaces of advanced design supersonic missiles.

The effect that forebody length has upon the force and moment coefficients was also examined. Computations show that the flowfield fully recovers at an axial position of six nosecone lengths aft of the nosetip.

Appendix: Development of the Shape Factor Parameter a

Parameter a quantifies the cross-sectional shape of the missile forebody fuselage. At $a = 0$, the shape is circular and at $a = 1$, the shape is sharp-cornered, i.e., a sharp-cornered square. Figure A1 shows the relationship between shape factor and the geometry of the cross section. For the square cross sections, the circular fillet, defined by R_f, is scribed over an arc of 90 deg. For the triangular cross sections, R_f is scribed over a 120 deg arc. For the circular cross section, the fillet scribes a circle. R_f and a' are defined in terms of the radius, R, of the inscribed circle

$$R = R_f + a' \tag{A1}$$

Thus one can write

$$(a'/R) + (R_f/R) = 1 \tag{A2}$$

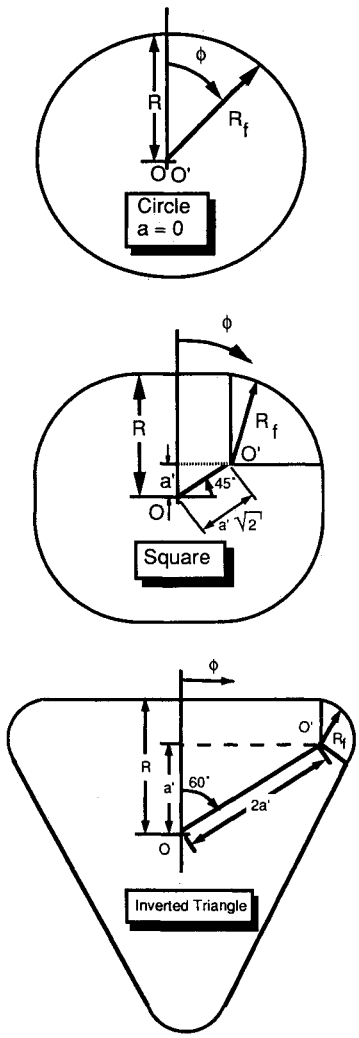

Fig. A1 Shape factor parameter definition for noncircular cross sections.

However, the parameter a is defined as a'/R so that,

$$a = 1 - (R_f/R) \tag{A3}$$

As a approaches 0, R_f approaches R and as a approaches 1, R_f approaches 0. This implies that all fuselage shapes collapse to an identical, circular cross section of radius R when a goes to zero. In this paper, R was constant (2.54 cm) for all the shapes, except the shapes used in the comparison with Ref. 5.

Acknowledgments

This work has been supported by McDonnell Douglas Missile Systems Company of St. Louis, Missouri through the Independent Research and Development Program, monitored by John E. Williams and Kurt D. Bausch. Additional funds were provided by the Missouri Research Assistance Act.

References

[1]Priolo, F. J., and Wardlaw, A. B., Jr., "Supersonic Non-Circular Missile Computations," AIAA Paper 88-0278, 26th Aerospace Sciences Meeting, Reno, NV, Jan. 1988.

[2]Nelson, H. F., "Wing-Body Interference Lift for Supersonic Missiles with Elliptic Cross-Section Fuselages," *Journal of Spacecraft and Rockets*, Vol. 26, No. 5, 1989, pp. 322–329.

[3]Sigal, A., and Lapidot, E., "The Aerodynamic Characteristics of Configurations Having Bodies with Square, Rectangular, and Circular Cross-Sections at a Mach Number of 0.75," AIAA Paper 87-

2429, 1987.

[4]Hutt, G. R., and Howe, A. J., "Effects of Cross Section and Nose Geometry on Slender-Body Supersonic Aerodynamics," *Journal of Spacecraft and Rockets,* Vol. 25, No. 2, 1988, pp. 189–193.

[5]Carlson, H. W., and Gapcynski, J. P., "An Experimental Investigation At a Mach Number of 2.01 of the Effects of Body Cross-Section Shape On the Aerodynamic Characteristics of Bodies and Wing-Body Combinations," NACA RM L55E23, July 1955.

[6]Jorgensen, L. H., "Inclined Bodies of Various Cross Sections at Supersonic Speeds," NASA Memo 10-3-58A, Nov. 1958.

[7]Sigal, A., "Analysis Methods and Experiments for Missiles with Noncircular Fuselages," *Tactical Missile Aerodynamics,* edited by M. R. Mendenhall. Progress in Astronautics and Aeronautics Series, AIAA, Washington, DC (to be published).

[8]Schindel, L. H., "Effects of Vortex Separation on the Lift Distribution on Bodies of Elliptic Cross Section," *Journal of Aircraft,* Vol. 6, No. 6, 1969, pp. 537–543.

[9]Wardlaw, A. B., Jr., and Davis, S. F., "Euler Solutions for Delta Wings," AIAA Paper 89-3398-CP, 1989.

[10]Siclari, M. J., and Del Guidice, P., "Hybrid Finite Volume Approach to Euler Solutions in Supersonic Flows," *AIAA Journal,* Vol. 28, No. 1, 1990, pp. 66–74.

[11]Priolo, F. J., and Wardlaw, A. B., Jr., "Euler Space-Marching Computations with Crossflow Separation for Missile-Type Bodies," AIAA Paper 90-0616, 28th Aerospace Sciences Meeting, Reno, NV, Jan. 1990.

[12]Hall, D. W., Hines, R. W., Baltakis, F. P., and Wardlaw, A. B., Jr., "Coupled Inviscid/Viscous Aerodynamic Predictions for Supersonic Tactical Missiles," AIAA Paper 90-0617, 28th Aerospace Sciences Meeting, Reno, NV, Jan. 1990.

[13]Lijewski, L. E., "Transonic Euler Solutions on a Blunt, Body-Wing-Canard Configuration," *Journal of Spacecraft and Rockets,* Vol. 25, No. 6, 1988, pp. 393–399.

[14]Miller, D. S., and Wood, R. M., "Leeside Flows over Delta Wings at Supersonic Speeds," *Journal of Aircraft,* Vol. 21, No. 9, 1984, pp. 680–686.

[15]Muller, B., and Rizzi, A., "Navier-Stokes Computation of Transonic Vortices Over a Rounding Leading Edge Delta Wing," AIAA Paper 87-1227, AIAA 19th Fluid Dynamics, Plasma Dynamics, and Lasers Conf., June 1987.

[16]Ying, S. X., Schiff, L. B., and Steger, J. L., "A Numerical Study of Three-Dimensional Seperated Flow Past a Hemisphere Cylinder," AIAA Paper 87-1207, AIAA 19th Fluid Dynamics, Plasma Dynamics, and Laser Conf., June 1987.

[17]Fujii, K., and Schiff, L. B., "Numerical Simulation of Vortical Flows Over a Strake-Delta Wing," AIAA Paper 87-1229, AIAA 19th Fluid Dynamics, Plasma Dynamic, and Lasers Conf., June 1987.

[18]Payne, F. M., Ng, T. T., and Nelson, R. C., "Experimental Study of the Velocity Field on a Delta Wing," AIAA Paper 87-1231, AIAA 19th Fluid Dynamics, Plasma Dynamics, and Lasers Conf., June 1987.

[19]Erickson, G. E., and Rogers, L. W., "Experimental Study of the Vortex Flow Behavior on a Generic Fighter Wing at Subsonic and Transonic Speeds," AIAA Paper 87-1262, AIAA 19th Fluid Dynamics, Plasma Dynamics, and Lasers Conf., June 1987.

[20]Ward, K. C., and Katz, J., "A Flow Visualization Study of the Vortex Structures Around an Inclined Body of Revolution," AIAA Paper 87-1247, AIAA 19th Fluid Dynamics, Plasma Dynamics, and Laser Conf., June 1987.

[21]Ayoub, A., and McLachlan, B. G., "Slender Delta Wing at High Angles of Attack—a Flow Visualization Study," AIAA Paper 87-1230, AIAA 19th Fluid Dynamics, Plasma Dynamics, and Lasers Conf., June 1987.

[22]Wardlaw, A. B., Jr., and Davis, S. F., "A Second Order Godunov Method for Tactical Missiles," Naval Surface Weapons Center, NSWC TR 86-506, Dec. 1986.

[23]Wardlaw, A. B., Jr., and Priolo, F. J., "Applying the ZEUS Code," Naval Surface Weapons Center, NSWC TR 86-508, Dec. 1986.

[24]Wardlaw, A. B., Jr., Priolo, F. J., and Solomon, J. M., "Multiple-Zone Strategy for Supersonic Missiles," *Journal of Spacecraft and Rockets,* Vol. 24, No. 4, 1987, pp. 377–384.

[25]Wardlaw, A. B., Jr., Baltakis, F. P., Martin, F. M., Priolo, F. J., and Jettmar, R. U., "A Godunov Method for Supersonic Tactical Missiles," *Journal of Spacecraft and Rockets,* Vol. 24, No. 1, 1987, pp. 40–47.

[26]Bausch, K. D., Personal communication, Feb. 1990.

[27]Est, B. E., and Nelson, H. F., "Supersonic Aerodynamics of Noncircular Cross Section Missile Forebodies," AIAA Paper 91-0390, AIAA 29th Aerospace Sciences Meeting, Jan. 1991.

[28]Est, B. E., "Computational Aerodynamics of Supersonic Missiles with Noncircular Cross Section," M.S. Thesis, Dept. of Mechanical and Aerospace Engineering and Engineering Mechanics, Univ. of Missouri-Rolla, May 1991.

[29]Polhamus, E. C., Geller, E. W., and Grunwald, "Pressure and Force Characteristics of Noncircular Cylinders as Affected by Reynolds Number with a Method Included for Determining the Potential Flow about Arbitrary Shapes," NACA Technical Rept. R-46, Langley Research Center, 1959.